J|A|C|S ARTICLES

Published on Web 11/19/2010

Sol−Gel Synthesis, Electrochemical Characterization, and Stability Testing of $Ti_{0.7}W_{0.3}O_2$ Nanoparticles for Catalyst Support Applications in Proton-Exchange Membrane Fuel Cells

Chinmayee V. Subban,[‡] Qin Zhou,[‡] Anthony Hu,[‡] Thomas E. Moylan,[†] Frederick T. Wagner,[†] and Francis J. DiSalvo[‡,*]

Department of Chemistry and Chemical Biology, Cornell University, Ithaca, New York 14853, United States, and Electrochemical Energy Research Lab, General Motors Research and Development, Warren, Michigan 48090, and Honeoye Falls, New York 14472, United States

Received August 17, 2010; E-mail: fjd3@cornell.edu

Abstract: The materials currently used in proton-exchange membrane fuel cells (PEMFCs) require complex control of operating conditions to make them sufficiently durable to permit commercial deployment. One of the major materials challenges to allow simplification of fuel cell operating strategies is the discovery of catalyst supports that are much more stable to oxidative decomposition than currently used carbon blacks. Here we report the synthesis and characterization of $Ti_{0.7}W_{0.3}O_2$ nanoparticles (approximately 50 nm diameter), a promising doped metal oxide that is a candidate for such a durable catalyst support. The synthesized nanoparticles were platinized, characterized by electrochemical testing, and evaluated for stability under PEMFC and other oxidizing acidic conditions. $Ti_{0.7}W_{0.3}O_2$ nanoparticles show no evidence of decomposition when heated in a Nafion solution for 3 weeks at 80 °C. In contrast, when heated in sulfuric, nitric, perchloric, or hydrochloric acid, the oxide reacts to form salts such as titanylsulfatehydrate from sulfuric acid. Electrochemical tests show that rates of hydrogen oxidation and oxygen reduction by platinum nanoparticles supported on $Ti_{0.7}W_{0.3}O_2$ are comparable to those of commercial Pt on carbon black.

Introduction

Fuel cells were invented in 1839 by Sir William Grove.[1] Unlike the internal combustion engine, the efficiency of fuel cells is not subject to the Carnot limit, since they are not heat engines. Calculations suggest the possibility of free energy conversion efficiencies of perhaps 90% in fuel cells, though the limited kinetics of the oxygen reduction reaction (ORR) have restricted the achieved efficiencies to lower values. The promises of high efficiency, low regulated emissions, and (with a proper energy chain) low greenhouse gas emissions have made fuel cells an attractive research and development objective as an alternative to current energy conversion technologies.[2,3]

There are various types of fuel cells, based on the temperature of operation, fuels that can be used, and components such as the electrolyte. However, the proton-exchange membrane fuel cell (PEMFC) is of interest for many applications, including portable electronics and automobiles, due to its low temperature of operation and fast start−stop capabilities.[4]

The materials currently used in PEMFCs require complex control schemes and associated hardware to achieve adequate durability.[5] The catalyst support, electrodes, and membrane can undergo chemical degradation, especially after many start−stop cycles, if operating conditions are not tightly controlled. Furthermore, the catalyst is expensive and easily poisoned. Hence, there are several materials challenges associated with each component of the membrane electrode assembly, the core of a PEMFC. This work is focused on the synthesis and characterization of more durable catalyst supports.

Current PEMFC technology uses carbon black as a catalyst support because it offers two important characteristics: (i) sufficient electronic conductivity to transport charge to and from the catalyst (at least 0.1 S/cm)[6] and (ii) a morphology with open porosity for movement of fuel, oxidant, and product species. Further, carbon black particles (50−100 nm) have been developed to bind 3−5 nm platinum or platinum-based catalyst nanoparticles. In particular, one form of carbon black commonly used is VulcanXC-72.[5] However, as a catalyst support, these

[‡] Cornell University.
[†] General Motors Research and Development.

(1) Grove, W. *Philos. Mag., Ser. 3* **1839**, *14*, 127.
(2) Bagotsky, V. S. *Fuel Cells: Problems and Solutions*; Wiley: New York, 2009.
(3) Borup, R.; et al. *Chem. Rev.* **2007**, *107*, 3904–3951.
(4) O'Hayre, R. P. *Fuel cell fundamentals*; John Wiley & Sons: Hoboken, NJ, 2009.
(5) Mathias, M. F.; Makharia, R.; Gasteiger, H. A.; Conley, J. J.; Fuller, T. J.; Gittleman, C. I.; Kocha, S. S.; Miller, D. P.; Mittelsteadt, C. K.; Xie, T.; Yan, S. G.; Yu, P. T. *Electrochem. Soc. Interface* **2005**, *14*, 24–35.
(6) Wagner, F. T.; Yan, S. G.; Yu, P. T. In *Handbook of Fuel Cells: Fundamentals, Technology and Applications*; Vielstich, W., Yokokawa, H., Gasteiger, H. A., Eds.; John Wiley &Sons, Ltd.: Chichester, UK, 2009; Vol. 5, pp 250−263.

carbons corrode too rapidly, especially under inadequately controlled transient-load and on/off operation conditions.[2,3,5,7,8]

PEMFCs function at low pH (1−2), and the cathode electrode can experience potentials up to +1.5 V vs the normal hydrogen electrode (NHE) under fuel starvation.[2] No nonprecious metal is thermodynamically stable at all these potentials in acidic aqueous media.[9] Sulfides, carbides, and nitrides are all thermodynamically driven to oxidize or hydrolyze to oxides, at least at the surface, under these conditions. However, some oxides with metals in their highest oxidation state demonstrate good stability in air/water mixtures. But under some conditions (pH ≠ 7, elevated temperature, with other ions in solution, applied potential, etc.), surface reactions can occur. Such reactions take on even more importance in nanoscale materials, due to the high ratio of surface to bulk atoms.

There are few oxides that demonstrate structural and chemical stability at the potentials and pH of interest: TiO_2, Nb_2O_5, Ta_2O_5, and WO_3.[9] Unfortunately, since in each case the metal is in its highest oxidation state, none of these oxides are conducting. However, these oxides can be partially reduced[10−12] or doped with other metal cations,[13−23] resulting in metallic or semiconducting behavior. For example, it is known that rutile (TiO_2) can be doped with other cations to prepare $Ti_{1-x}M_xO_2$, where M is a metal from group V or greater.[13−23] Also, according to Pourbaix diagrams,[9] TiO_2 is highly stable in water over a broad range of pH values (−1 to 14) and from low to high potential (pH-dependent). Hence, doped TiO_2 has the possibility of being both electrically conducting and kinetically stable under fuel cell conditions, assuming that the doping does not radically alter the chemical stability of the host lattice. Some transition metal oxides have been studied as electrodes or supports in a variety of electrochemical systems.[12,23−27]

Rutile has a tetragonal structure and is a large-band-gap semiconductor (3.0−3.5 eV).[28,29] Since pure titania has very few charge carriers, resulting in low electronic conductivity, conductivity must be achieved either by aleovalent cation substitution or by introduction of oxygen vacancies. On the other hand, WO_2 is a conductive material with a distorted rutile structure resulting from W−W bonding,[30] but it is thermodynamically stable only over a narrow range of potentials (around −0.1 V).[9] However, when WO_2 is doped into TiO_2, especially at low concentrations, a chemically stable and conductive system can be obtained. Though the expected percolation limit for near-neighbor W−O−W connectivity is near $x = 0.5$ (where x is the mole fraction of WO_2 in TiO_2),[31] DFT calculations predict metallic conductivity from overlap of occupied W 5d orbitals with orbitals of neighboring O and Ti[32] even at much lower concentrations of W. Fuel cell technologists have proposed a modest target for the minimum conductivity of new catalyst supports of 0.1 S/cm[6]. Initial high-temperature synthesis experiments suggested that this target could easily be met with 30% W doping.[33] Further, W has the advantage over other doping elements (e.g., Nb) in that W−W pairing does not cause complete localization of the electrons.

In this paper, the $Ti_{0.7}W_{0.3}O_2$ system is discussed. We report the sol−gel synthesis of nanoparticles and their electrochemical behavior. We are currently examining the use of other dopants in TiO_2 as well as other oxide hosts for catalyst support applications, but these topics will not be discussed here.

Experimental Section

$Ti_{1-x}W_xO_2$ has been successfully synthesized through traditional solid-state techniques. These involve high temperature (1100 °C) and long reaction times, and they result in micrometer-size particles[33] which are too large to be used as catalyst supports. The sol−gel technique is widely used for the synthesis of mixed-metal oxides, giving atomic-scale mixing that enables lower calcination temperatures, resulting in high-purity, single-phase, mixed-cation oxides at low temperature.[35] Hence, in order to produce 50 −100 nm nanoparticles of the desired composition, a sol−gel based multistep process has been developed. The process is a variation of traditional Pechini synthesis,[34,35] involving *in situ* polymerization of citric acid and ethylene glycol.

Materials. Titanium tetra-isopropoxide was purchased from Gelest; citric acid from Fisher Scientific; tungsten hexa-ethoxide, Zr foil (0.025 mm thick, annealed), and anhydrous ethylene glycol (ACS, spectroscopic grade) from Alfa Aesar; anhydrous ethanol (ACS grade) from Pharmco Aaper; and Nafion (5 wt % in lower aliphatic alcohols and water) from Sigma-Aldrich.

Synthesis. Titanium tetra-isopropoxide (0.52 mL) and ethylene glycol (0.14 mL) were added to 10 mL of ethanol each, while tungsten hexa-ethoxide (0.34 g) and citric acid (0.96 g) were dissolved in 45 and 15 mL of anhydrous ethanol, respectively. The

(7) Cheng, X.; Shi, Z.; Glass, N.; Zhang, L.; Zhang, J.; Song, D.; Liu, Z.-S.; Wang, H.; Shen, J. *J. Power Sources* **2007**, *165*, 739–756.
(8) Gasteiger, H. A. *Electrochemistry* **2007**, *75*, 103.
(9) Pourbaix, M., National Association of Corrosion Engineers, 1974.
(10) Inglis, A. D.; Lepage, Y.; Strobel, P.; Hurd, C. M. *J. Phys. C−Solid State Phys.* **1983**, *16*, 317–333.
(11) Ioroi, T.; Senoh, H.; Yamazaki, S. I.; Siroma, Z.; Fujiwara, N.; Yasuda, K. *J. Electrochem. Soc.* **2008**, *155*, B321–B326.
(12) Ioroi, T.; Siroma, Z.; Fujiwara, N.; Yamazaki, S.; Yasuda, K. *Electrochem. Commun.* **2005**, *7*, 183–188.
(13) Chang, L. L. Y. *J. Am. Ceram. Soc.* **1968**, *51*, 295.
(14) Chen, G. Y.; Waraksa, C. C.; Cho, H. G.; Macdonald, D. D.; Mallouk, T. E. *J. Electrochem. Soc.* **2003**, *150*, E423–E428.
(15) Colomer, M. T.; Velasco, M. J. *J. Eur. Ceram. Soc.* **2007**, *27*, 2369–2376.
(16) Garcia, B. L.; Fuentes, R.; Weidner, J. W. *Electrochem. Solid State Lett.* **2007**, *10*, B108–B110.
(17) Horkans, J.; Shafer, M. W. *J. Electrochem. Soc.* **1977**, *124*, 1202–1207.
(18) Murata, Y.; Fukuta, S.; Ishikawa, S. *Zairyo Kankyo* **2000**, *49*, 412–419.
(19) Pejryd, L. *J. Am. Ceram. Soc.* **1986**, *69*, 717–720.
(20) Roy, A.; Dey, S.; Ghose, J. *Indian J. Phys., A* **2000**, *74A*, 191–193.
(21) Sakata, K.; Nishida, I.; Matsushi, M.; Sakata, T. *J. Phys. Soc. Jpn.* **1969**, *27*, 506.
(22) Sasaki, K.; Zhang, L.; Adzic, R. R. *Phys. Chem. Chem. Phys.* **2008**, *10*, 159–167.
(23) Smith, J. R.; Walsh, F. C.; Clarke, R. L. *J. Appl. Electrochem.* **1998**, *28*, 1021–1033.
(24) Harris, L. A.; Gerstner, M. E.; Wilson, R. H. *J. Electrochem. Soc.* **1979**, *126*, 850–855.
(25) Huang, S. Y.; Ganesan, P.; Park, S.; Popov, B. N. *J. Am. Chem. Soc.* **2009**, *131*, 13898.
(26) Rajalakshmi, N.; Lakshmi, N.; Dhathathreyan, K. S. *Int. J. Hydrogen Energy* **2008**, *33*, 7521–7526.
(27) Wilson, R. H.; Harris, L. A.; Gerstner, M. E. *J. Electrochem. Soc.* **1979**, *126*, 844–850.
(28) Ashour, A. *Surf. Rev. Lett.* **2006**, *13*, 87–92.
(29) Mikami, M.; Nakamura, S.; Kitao, O.; Arakawa, H.; Gonze, X. *Jpn. J. Appl. Phys. Part 2−Letters* **2000**, *39*, L847–L850.
(30) Palmer, D. J.; Dickens, P. G. *Acta Crystallogr.* **1979**, *B35*, 2199–2201.
(31) Zallen, R. The Percolation Model. *The Physics of Amorphous Solids*; John Wiley and Sons: New York, NY, 1983; Chapter 4, p304.
(32) Aryanpour, M.; Hoffmann, R.; DiSalvo, F. J. *Chem. Mater.* **2009**, *21*, 1627–1635.
(33) Subban, C.; Zhou, Q.; Leonard, B.; Ranjan, C.; Edvenson, H. M.; Munie, S.; Hunting, J.; DiSalvo, F. J. *Philos. Trans. R. Soc. A* **2010**, *368*, 3243–3253.
(34) Hui, W.; Jia-Heng, L., *J. Wuhan Univ. Technol.* **2002**, December (Material Science Edition).
(35) Niederberger, M.; Garnweitner, G. *Chem.−Eur. J.* **2006**, *12*, 7282–7302.

solutions were then mixed together on a Schlenk line under air-free conditions, resulting in a 2:1:1 citric acid-to-metal-to-ethylene glycol molar ratio solution. The mixture was then exposed to air, poured into a Petri dish, and heated in air to evaporate the solvent and polymerize the citric acid and ethylene glycol at 75 °C for up to 12 h in a drying oven. The resulting clear gel was then calcined at 450 °C in air for 6 h. The calcined product is a free-flowing, white to light tan powder. At this point, the W is fully oxidized (6+) and needs to be reduced (4+). This was achieved by heating the calcined sample in a sealed, evacuated silica tube with stoichiometric amounts of Zr foil at 750 °C for up to 2 days.[36] The Zr metal is kept separate from the oxide by putting it in a small open silica tube. The Zr forms ZrO_2 on heating, thereby reducing the W from 6+ to 4+. $Ti_{0.7}W_{0.3}O_2$ is a black, free-flowing powder. A TGA scan of the calcined product was conducted prior to heating with Zr to quantify the water adsorbed on the relatively high surface area of the cool, air-exposed calcined material (generally close to 3.5 wt %) and to precisely determine the exact amount of Zr foil required to reduce the W^{6+} just to W^{4+}. All of the H_2O was carefully removed from the calcined material before sealing the tube by pumping under vacuum and gently heating until no increase in vacuum pressure was seen with further heating. The presence of H_2O not only would preclude the proper reduction of W, it also acts as a good W-transport agent at elevated temperatures[37] and would result in an inhomogeneous final product.

Characterization. The samples were characterized by powder X-ray diffraction using a Rigaku Ultima VI diffractometer. Scanning electron microscopy (SEM) and energy dispersive X-ray analysis (EDX) were performed using a LEO-1550 field emission SEM (FSEM). Thermogravimetric analysis (TGA) was conducted using a TA Instruments Q50. Tunneling electron microscopy (TEM) was conducted using a Tecnai F20 instrument, and a Horiba elemental analyzer (EMGA, EF-600) was used to determine the oxygen content.

Stability Tests. About 0.1 g of the $Ti_{0.7}W_{0.3}O_2$ nanopowder was placed in 4 mL of 3 M aqueous solutions of four different acids: H_2SO_4, HNO_3, HCl, $NaClO_4$/HCl. A fifth mixture was prepared in a 4 mL Nafion solution (5 wt %). All mixtures were held in glass vials at 80 °C (nominal PEMFC conditions) for up to 3 weeks.

Platinization. Platinization of the nanoscale powders using hydrazine was done at GM research laboratories according to the following procedure. About 1 g of $Ti_{0.7}W_{0.3}O_2$ was sonicated in 300 mL of H_2O, heated to 80 °C, and mixed with a solution of 1.6 g of $(NH_3)_2Pt(NO_2)_2$ in 100 mL of H_2O. This mixture was heated to 80 °C with CO bubbling at 400 sccm for up to 30 min with constant stirring. The pH of the solution was adjusted to 3 using acetic acid, and a solution of hydrazine (0.333 g in 10 mL of H_2O) was added. The mixture was stirred with CO bubbling at 80 °C for up to 3 h, and then stirring was continued overnight at room temperature. The final product was obtained by filtration and vacuum drying.

Electrochemical Testing. $Ti_{0.7}W_{0.3}O_2$. A stable suspension of the $Ti_{0.7}W_{0.3}O_2$ nanopowder was prepared by mixing 10 mg of the nanopowder, 3.98 mL of distilled water, 1 mL of isopropyl alcohol, and 20 μL of Nafion solution (5 wt % in alcohols and water) and sonicating for 2 h. About 20 μL of the suspension (200 μg of oxide cm^{-2}) of $Ti_{0.7}W_{0.3}O_2$ was applied to a polished 5 mm diameter glassy carbon electrode and dried in air for rotating disk electrode (RDE) electrochemical studies. A NaCl-saturated Ag/AgCl electrode and a carbon electrode were used as the reference and the counter electrode, respectively. Tests were conducted in a 0.1 M sulfuric acid solution saturated by Ar, O_2, and H_2, respectively.

Platinized $Ti_{0.7}W_{0.3}O_2$. The catalyst was mixed with 20 vol % 2-propanol and 4 wt % Nafion in water and sonicated to form an ink. A 20 μL aliquot of the dispersed ink was deposited onto a polished 5 mm diameter glassy carbon disk and allowed to dry under ambient air. Catalyst loadings were 25−35 $\mu g_{Pt}/cm^2_{geo}$ with 4−5 wt % Nafion in the dried film to act as a binder. For reference, similar methods were used to prepare RDEs using a 46 wt % Pt/Vulcan baseline catalyst (TEC10V50E from TKK).

A Pyrex cell was filled with about 100 mL of 0.1 M $HClO_4$ (prepared from concentrated $HClO_4$ from GFS Chemicals) and covered with a Teflon cap. A reversible hydrogen electrode (RHE) reference was placed in a separate beaker and connected to the cell by a bridge tube; and the beaker, bridge, and RHE were all filled with the same electrolyte. The counter electrode was a platinum mesh connected to the cell through a coarse glass frit. All potentials were referenced to the RHE.

The electrode film was immersed at open circuit as the electrolyte was being actively sparged with argon, and it was activated by cycling 400 times between 50 and 1100 mV at 1 V/s. Once the CV current was stabilized by the rapid cycling, three additional voltage sweeps were run at 20 mV/s. The Pt surface area was estimated by the adsorption charge of the underpotential-deposited (UPD) hydrogen assuming 210 $\mu C/cm^2_{Pt}$.

Oxygen was sparged for a minimum of 30 min initially to saturate the electrolyte and then continuously throughout the ORR measurement. With the electrode being rotated at 1600 rpm, the film was initially held at +150 mV for 60 s and then swept to +1100 mV at 5 mV/s. The geometric current measured at 900 mV is corrected using the diffusion current through the hydrodynamic boundary layer to estimate the kinetic current, $1/i_K = 1/i_{geo} - 1/i_{lim}$, and the catalyst activity was calculated from this kinetic current.

Results and Discussion

The powder X-ray diffraction pattern for the $Ti_{0.7}W_{0.3}O_2$ nanoparticles (Figure 1a) can be completely indexed with a tetragonal unit cell that is slightly shifted from pure TiO_2 due to doping with tungsten. The red lines indicate the peak positions for pure rutile TiO_2 (PDF no. 01-072-4812). Some peaks shift to higher values of 2θ, while others shift to lower values compared to pure rutile TiO_2. This behavior reveals an expansion of the *a*-axis and a contraction of the *c*-axis due to W−W pairing in the doped compound. Such pairing is also seen in WO_2 and is expected in the doped TiO_2.[30,32] The lattice parameters of pure TiO_2 are $a = 4.6021$ Å, $c = 2.9563$ Å, with $Z = 2$ and $V = 62.612$ Å^3. The whole powder pattern fitting (WPPF) technique was used to calculate the lattice parameters of $Ti_{0.7}W_{0.3}O_2$: $a = 4.683(1)$ Å, $c = 2.919(1)$ Å, $V = 63.87$ Å^3. As predicted by theory[32] and as seen in the high-temperature product,[33] the unit cell volume increases by about 2% with 30% W doping. The X-ray peaks are broad due to the nanoscale size crystallite domains and/or small compositional inhomogeneities. Assuming uniform composition, the crystallite domain sizes are calculated to be 29 ± 3 nm using the Williamson−Hall method.[38−40]

The samples were examined by SEM and EDX. Figure 1b illustrates closely packed particles on the surface of the flake-like morphology of the $Ti_{0.7}W_{0.3}O_2$, which results from the multistep synthesis in a Petri dish. Figure 1c shows a cross-section of the flake, highlighting an open network of smaller particles in the middle with more densely packed, larger particles on the edges. The robustness of the flakes suggests partial sintering of the particles, which results in the desired open

(36) Marezio, M.; Bordet, P.; Capponi, J. J.; Cava, R. J.; Chaillout, C.; Chenavas, J.; Hewat, A. W.; Hewat, E. A.; Hodeau, J. L.; Strobel, P. *Physica C: Supercond. Appl.* **1989**, 162−164, 281−284.
(37) Schafer, H. *Chemical Transport Reactions*; Academic Press: New York, 1964.
(38) Chatterjee, P.; Sen Gupta, S. P. *J. Appl. Crystallogr.* **1999**, *32*, 1060–1068.
(39) Gesenhues, U. *J. Appl. Crystallogr.* **2005**, *38*, 749–756.
(40) Pelleg, J.; Elish, E.; Mogilyanski, D. *Metallurg. Mater. Trans. a−Phys. Metallurgy Mater. Sci.* **2005**, *36A*, 3187–3194.

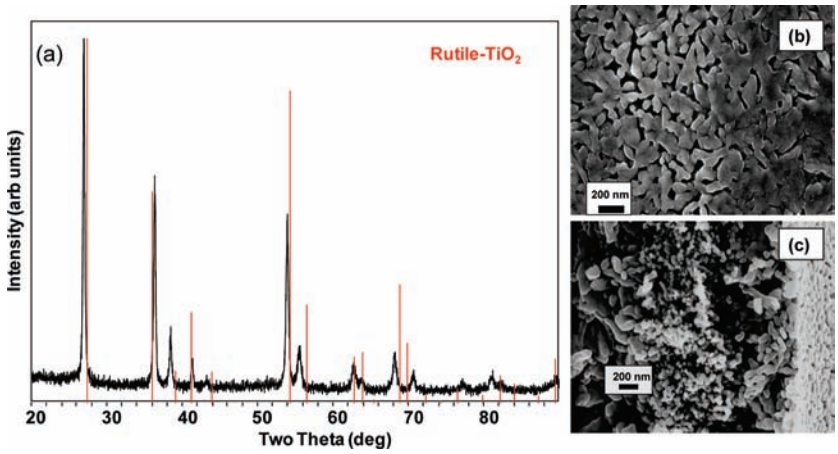

Figure 1. (a) Powder X-ray diffraction pattern for $Ti_{0.7}W_{0.3}O_2$. The red lines indicate peak positions for pure rutile TiO_2. Measured peaks are shifted due to W-doping. (b) SEM image showing the top surface of the flake-like morphology of the $Ti_{0.7}W_{0.3}O_2$ prepared by the sol−gel method outlined in the text. The particles form a well-connected network on the surface and are about 100−200 nm in size. (c) SEM image of a cross-section of the flake-like morphology, with smaller particles and higher porosity in the interior of the flake. The flake surface runs vertically on the right-hand side of the image.

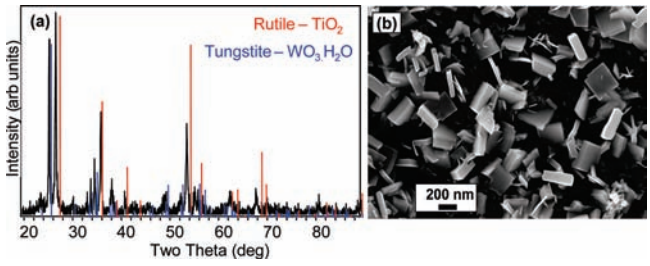

Figure 2. (a) X-ray diffraction pattern of $Ti_{0.7}W_{0.3}O_2$ nanopowder after treating with 3 M H_2SO_4 solution at 80 °C for 3 weeks. (b) SEM image of the acid-treated sample.

porosity. Synthesis design leading to the desired uniform particle size and open porosity of the oxide network is currently being optimized and will be the subject of a future publication. The average ratio of Ti to W was determined to about 2:1 through EDX. The oxygen content was measured using a combustion technique[41] before (29.2 ± 1 wt %) and after (25.5 ± 1 wt %) reducing the tungsten. These are quite close to the expected theoretical values of 29.3% and 26.5%, respectively.

The electrical conductivity of moderately compacted flakes of approximately 0.02 S/cm was obtained using a four-point probe, while a conductivity of about 0.9 S/cm was measured using a two-point probe. Some variability from method to method is expected due to different particle−particle contact resistances and differences in applied pressure distribution in the compaction.

The chemical stability of $Ti_{0.7}W_{0.3}O_2$ was tested in considerable stoichiometric excesses of various acids at 80 °C for up to 3 weeks. In H_2SO_4 or HNO_3, the tungsten was partially leached out and formed tungstite ($WO_3 \cdot H_2O$), while the TiO_2 formed either titanyl sulfate or titanyl nitrate.[42−44] Figure 2b shows the SEM micrograph of a $Ti_{0.7}W_{0.3}O_2$ sample treated with 3 M H_2SO_4 for 21 days at 80 °C. SEM images of samples treated in both hydrochloric acid and a mixture of $NaClO_4$ and HCl showed some needles of oxides of tungsten (by microprobe), but there were no noticeable changes in the X-ray patterns of these samples, indicating only slight reaction. Sulfuric and nitric acids are observed to be more aggressive than the other aqueous acids due to the formation of titanyl sulfate and titanyl nitrate complexes, exposing the tungsten to further oxidation, forming hydrates of WO_3. Interestingly, neither the X-ray pattern nor the SEM images of the sample treated with concentrated Nafion solution showed any changes (Figure 3). The reaction rate of the acids with the oxide was highest for sulfuric acid; however, the reaction was only about 50% complete even after 3 weeks at 80 °C. For application as a catalyst support in PEM fuel cells, stability in Nafion is essential; hence, $Ti_{0.7}W_{0.3}O_2$ appears to be a promising candidate on the basis of these results.

The electrochemical stability of $Ti_{0.7}W_{0.3}O_2$ nanopowders was examined under pH and applied potential conditions comparable to those of a fuel cell. The sample was tested, without any added Pt, over a potential range of 0.0−1.2 V vs RHE in 0.1 M sulfuric acid solution at room temperature. Since both the temperature and acid concentration are much lower than in the above stability tests, and since the electrochemical testing takes no more than a few hours, no evidence of corrosion of the oxide is seen. As shown in Figure 4a, when the sulfuric acid solution is degassed with argon, the oxide is not electrochemically active in the potential range of fuel cell operation (0 to +1.5 V vs RHE), suggesting a stable surface. Electrocatalytic activity tests revealed the onset of a low level of oxygen reduction at about −200 mV, and peaks for hydrogen evolution were noticed below −800 mV (Figure 4a). Generally, a material with activity for hydrogen evolution can also catalyze hydrogen oxidation; hence, the sample was tested for activity toward hydrogen oxidation. As seen in Figure 4b, the sample shows a small activity for hydrogen oxidation. It is important to notice that, in both the hydrogen oxidation reaction (HOR) and oxygen reduction reaction (ORR), the CV results are reproducible after multiple cycles, which indicates the electrochemical stability of the $Ti_{0.7}W_{0.3}O_2$ nanopowders. However, the onset potentials for HOR and ORR are much too low to be of interest for application of the material as a fuel cell electrocatalyst rather than as a support. Nevertheless, these data confirm at least short-term

(41) Kikkawa, S.; Nagasaka, K.; Takeda, T.; Bailey, M.; Sakurai, T.; Miyamoto, Y. *J. Solid State Chem.* **2007**, *180*, 1984–1989.
(42) Jablonski, M. *J. Therm. Anal. Calorim.* **2008**, *93* (3), 717−720.
(43) Kolen'ko, Y. V.; Burukhin, A. A.; Churagulov, B. R.; Oleinikov, N. N. *Inorg. Mater.* **2004**, *40*, 822–828.
(44) Sivakumar, S.; Pillai, P. K.; Mukundan, P.; Warrier, K. G. K. *Mater. Lett.* **2002**, *57*, 330–335.

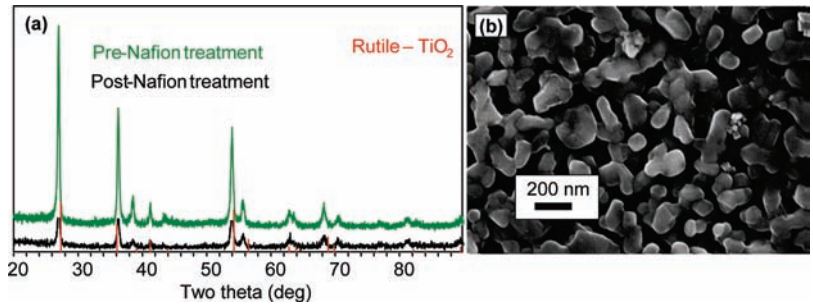

Figure 3. (a) X-ray diffraction pattern comparing $Ti_{0.7}W_{0.3}O_2$ nanopowder before and after treating with Nafion solution at 80 °C for 3 weeks. (b) SEM image of the sample post-treatment. The intensity of the Nafion-treated sample is low due to the small mass of the sample.

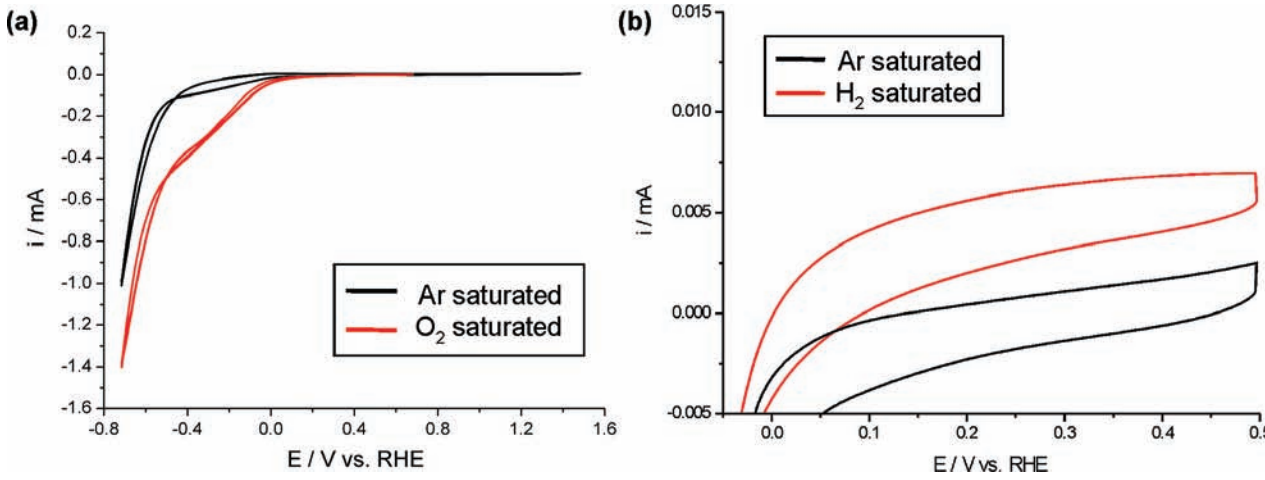

Figure 4. Electrochemical behavior of $Ti_{0.7}W_{0.3}O_2$-coated glassy carbon electrode: (a) oxygen- and argon-saturated and (b) hydrogen- and argon-saturated in 0.1 M H_2SO_4 (scan rate, 10 mV/s; rotating rate, 2000 rpm).

(meta) stability of $Ti_{0.7}W_{0.3}O_2$ in the potential range of fuel cell operation. The results for oxide nanoparticles with lower W-doping are provided in the Supporting Information.

In order to compare $Ti_{0.7}W_{0.3}O_2$ with the commercially used carbon black, the sample was coated with platinum nanoparticles following industry protocols and tested for oxygen reduction using a RDE technique. Figure 5a compares the X-ray diffraction pattern before and after deposition of Pt nanoparticles, and the various Pt peaks are easily distinguished. Further, the distribution of Pt nanoparticles was examined through TEM, and, as evident in Figure 5b, the Pt nanoparticles aggregate on the surface of the oxide. Figure 5c is a TEM image of one of the larger Pt aggregates. Nonetheless, after the deposition of Pt nanoparticles, the material showed a typical CV of Pt (Figure 6a), in which the hydrogen and "oxide" electrosorption/desorption regions were clearly visible. The CV curves confirmed the presence of electrochemically active (i.e., electrically connected) Pt on the surface of the oxide; however, the electrochemically active surface area of Pt on $Ti_{0.7}W_{0.3}O_2$ (24 m^2/g Pt) was lower than that on Vulcan (61 m^2/g Pt). This could be either a result of insufficient electrical conductivity of $Ti_{0.7}W_{0.3}O_2$ (0.02 to 0.9 S/cm, vs 2 S/cm for Vulcan) or due to aggregation of Pt particles. Although this Pt deposition technique is currently used for carbon black, it may still require optimization for oxide supports.

Figure 6b shows positive-going scans of RDEs coated with $Pt/Ti_{0.7}W_{0.3}O_{0.2}$ and Pt/Vulcan. Roughly comparable currents were obtained for the two electrodes, but the $Pt/Ti_{0.7}W_{0.3}O_{0.2}$ electrode contained 1.7 times the amount of the Pt on the Pt/Vulcan electrode. From the data at 0.9 V RHE, corrected for the diffusion-limited currents at low potentials, one calculates Pt-mass activities of 0.05 A/mg_{Pt} for the $Pt/Ti_{0.7}W_{0.3}O_{0.2}$ and 0.09 A/mg_{Pt} for the Pt/Vulcan. The Pt area-specific activities were 200 $\mu A/cm^2_{Pt}$ for the $Pt/Ti_{0.7}W_{0.3}O_{0.2}$ and 150 $\mu A/cm^2_{Pt}$ for the Pt/Vulcan. Even though the electrode preparation and testing methods were not reoptimized for the oxide support, the oxide-supported catalyst showed initial activity roughly comparable to that of standard Pt/Vulcan.

Conclusions

A useful material step toward improving durability in simplified proton exchange membrane fuel cell (PEMFC) systems is a catalyst support which is not susceptible to oxidative degradation, unlike the currently used carbon blacks. We successfully synthesized $Ti_{0.7}W_{0.3}O_2$ nanoparticles using a sol−gel technique and demonstrated their short-term electrochemical and chemical stability under conditions comparable to those in a PEMFC. Furthermore, these oxide nanopowders were successfully platinized, and the resulting electrochemical tests show oxygen reduction rates comparable to that of commercial Pt on carbon black. The activity per unit Pt surface area on $Ti_{0.7}W_{0.3}O_2$ (200 $\mu A/cm^2_{Pt}$) was comparable to that on Pt/Vulcan (150 $\mu A/cm^2_{Pt}$), but the mass activity of $Pt/Ti_{0.7}W_{0.3}O_2$ (0.05 A/mg_{Pt}) was lower than that of Pt/Vulcan (0.09 A/mg_{Pt}) due to the lower specific surface area. These results are very promising, considering that the electrical conductivity of the oxide (0.02−0.9 S/cm) is quite low compared to that of Vulcan (2 S/cm). Further work to characterize the functional durability of such supports in complete fuel cells is planned. Ongoing experiments are

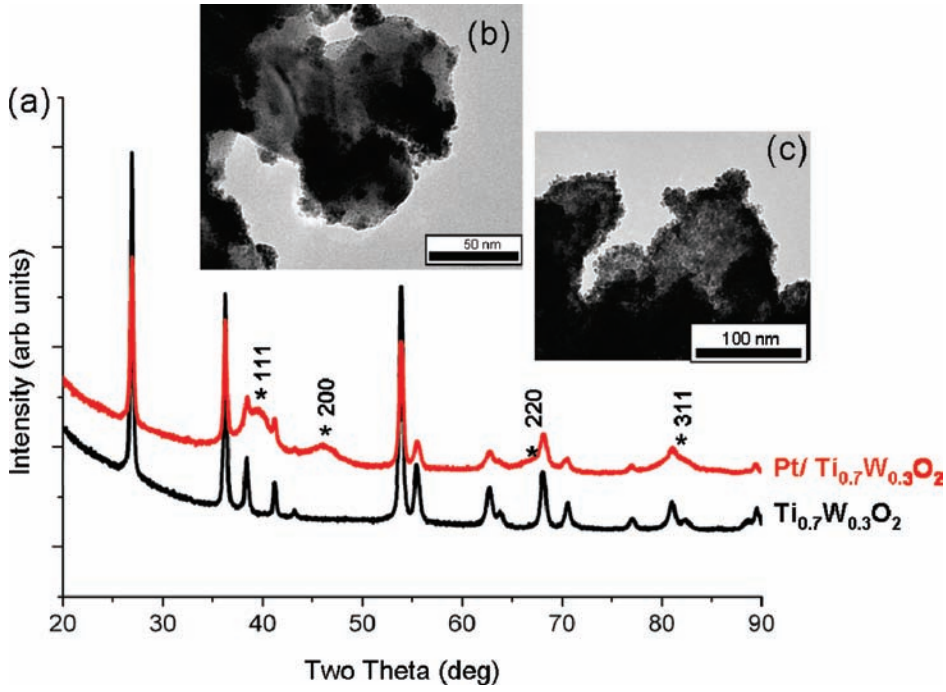

Figure 5. (a) X-ray diffraction patterns for $Ti_{0.7}W_{0.3}O_2$ and $Pt/Ti_{0.7}W_{0.3}O_2$ (39 wt %), with Pt peaks identified with asterisks and corresponding *hkl* values. Pt nanoparticles were deposited using the hydrazine reduction method. (b) TEM image showing aggregates of Pt nanoparticles on the surface of $Ti_{0.7}W_{0.3}O_2$. (c) TEM image of one of the larger Pt aggregates.

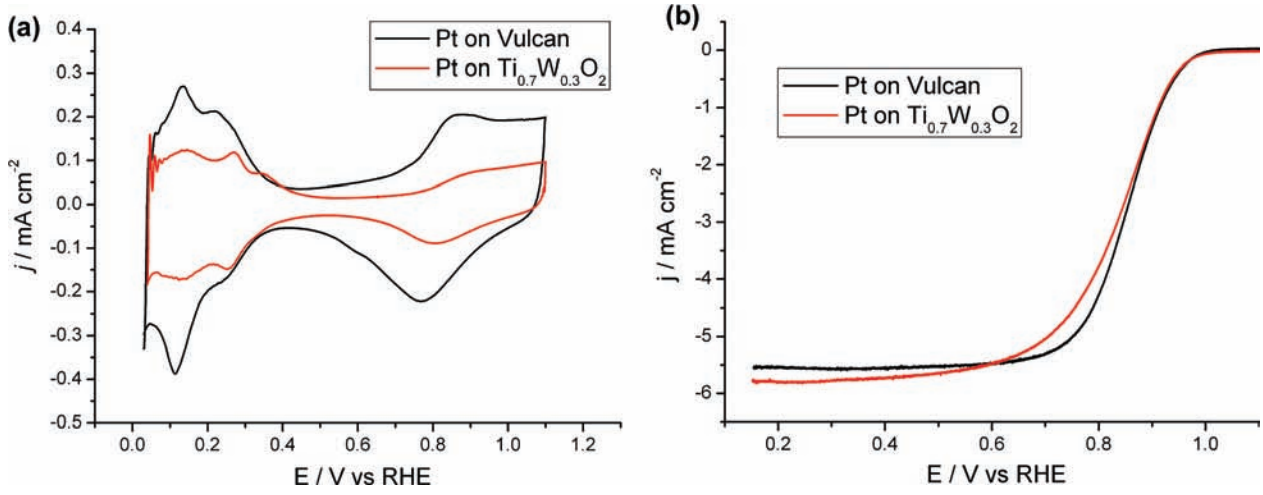

Figure 6. Comparison of platinized Vulcan (46 wt % Pt, 20.6 $\mu g_{Pt}/cm^2$, 61 m^2_{Pt}/g_{Pt}) and $Ti_{0.7}W_{0.3}O_2$ (39 wt % Pt, 34.6 $\mu g_{Pt}/cm^2$, 24 m^2_{Pt}/g_{Pt}). (a) Cyclic voltammogram and (b) oxygen reduction rates tested in an oxygen-saturated solution using a RDE. The active Pt specific surface area on the oxide was significantly lower than that of platinized Vulcan, and the Pt mass-specific activity of the $Pt/Ti_{0.7}W_{0.3}O_2$ was within a factor of 2 of that of the Pt/Vulcan.

aimed at increasing the conductivity, optimizing the open porosity, and testing the longer term stability of doped oxides based on TiO_2 and other early transition metal oxides.

Acknowledgment. This work was supported by the Department of Energy though grant DE-FG02-87ER45298, by Energy Materials Center at Cornell, an Energy Frontier Research Center funded by the U.S. Department of Energy, Office of Science, Office of Basic Energy Sciences under Award No. DE-SC0001086, and by a collaborative grant with General Motors Fuel Cell Activities in Honeoye Falls, NY, through the New York State Energy and Research Development Authority (Project 50815). Mohammed Atwan of Trison Business Solutions platinized the oxide supports at GM R&D following a method established by J. T. Johnson of the Chemical and Environmental Sciences Lab of GM R&D. Oxygen content measurements were conducted by Profs. Kikkawa and Masubuchi of Hokkaido University, Japan. Thanks to Dr. Brian Leonard for TEM assistance and to Dr. Akira Miura for helpful discussions. This work made use of SEM and TEM facilities of the Cornell Center for Materials Research (CCMR) with support from the National Science Foundation Materials Research Science and Engineering Centers (MRSEC) program (DMR 0520404).

Supporting Information Available: Details of varying W concentration, determination of elemental composition, and complete ref 3. This material is available free of charge via the Internet at http://pubs.acs.org.

JA1074163